Xu and Chisholm Supplemental Information

C. elegans epidermal wounding induces a mitochondrial ROS burst that promotes wound repair

Suhong Xu and Andrew D. Chisholm

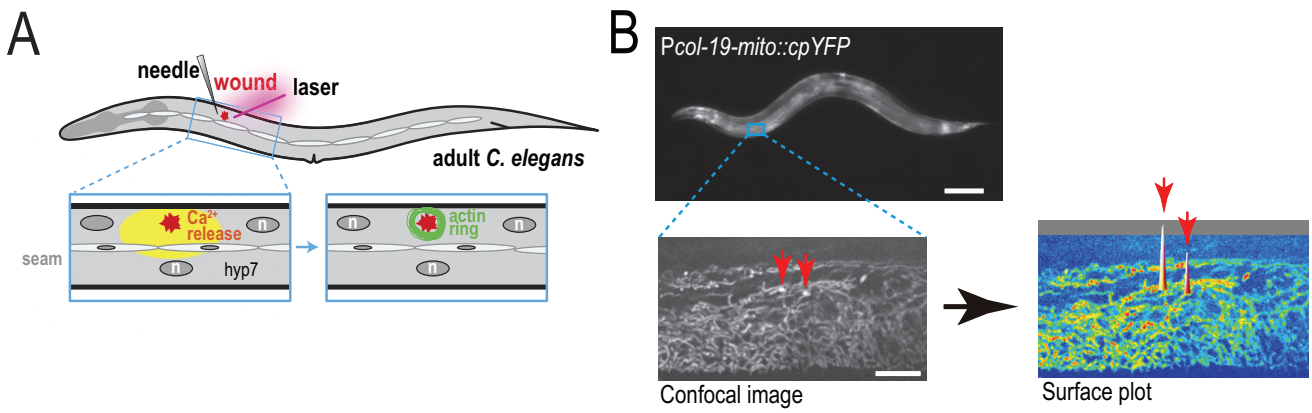
A
needle
wound
laser
adult C. elegans
seam
Ca2+ release
hyp7
actin ring
B
Pcol-19-mito::cpYFP
Confocal image
Surface plot

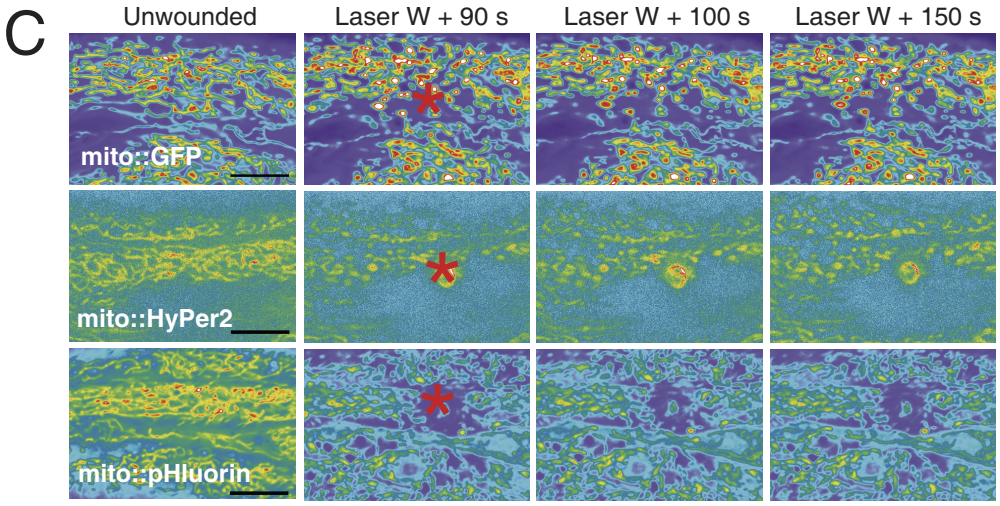
C
Unwounded
Laser W + 90 s
Laser W + 100 s
Laser W + 150 s
mito::GFP
mito::HyPer2
mito::pHluorin

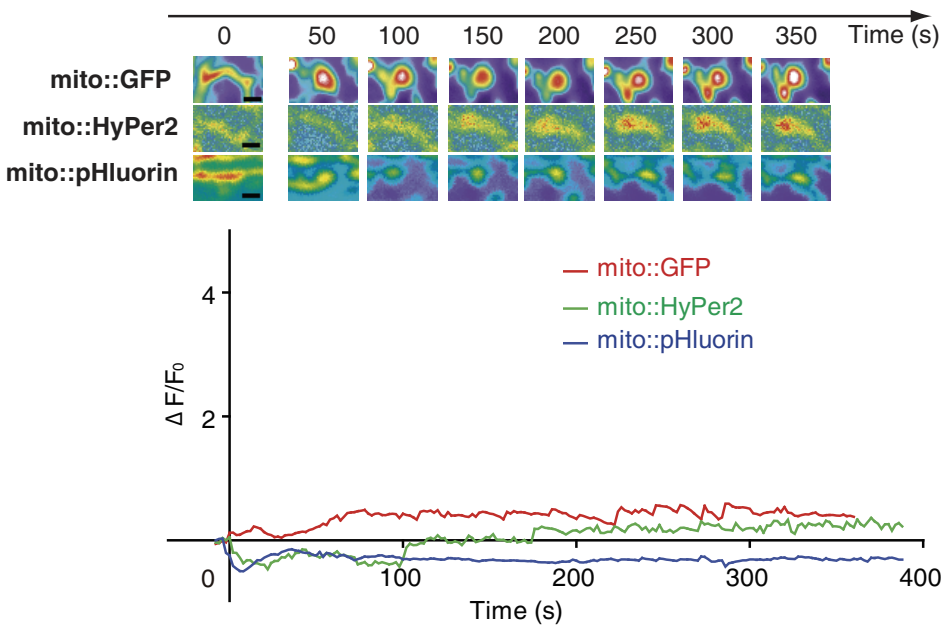
D
0
50
100
150
200
250
300
350
Time (s)
mito::GFP
mito::HyPer2
mito::pHluorin
mito::GFP
mito::HyPer2
mito::pHluorin
Δ F/F0
4
2
0
100
200
300
400
Time (s)

Figure S1

Supplemental Figures

Figure S1. *C. elegans* epidermal wounding induced mitoflashes are not due to changes in mitochondrial pH or H_2O_2, related to Figure 1.

(A) Diagram of the *C. elegans* skin wound repair assay. Wounds are induced in the lateral syncytial epidermal cell hyp7 by needle puncture or laser irradiation, inducing a rapid rise in cytosolic Ca^{2+} that triggers formation of F-actin rings at the wound site.

(B) Mitochondrial ROS (superoxide) are visualized with genetically encoded sensor cpYFP, targeted into the epidermal mitochondria by the Cox8 mitochondrial signal sequence ("mito") under the control of *col-19* promoter. The mito::cpYFP fluorescence signals were examined using spinning disk confocal microscopy and mitoflashes analyzed as surface plots using ImageJ. Scales, top: 100 μm, middle: 10 μm.

(C) Mitochondrially targeted GFP and HyPer2 or pHluorin sensors do not show flash-like dynamics after wounding. Representative spinning disk confocal images of mito::GFP, mito::HyPer2 (hydrogen peroxide sensor; YFP with 491 nm excitation shown) and mito::pHluorin (pH sensor) after laser wounding. All sensors are expressed in adult epidermis using the *col-19* promoter. Intensity color code; scale, 10 μm. Red asterisk indicates wound site.

(D) Top: Frames showing single mitochondria labeled either with mito::GFP, mito::HyPer2, or mito::pHluorin upon wounding. Intensity color code; scale, 1 μm. Bottom: representative traces of mito::GFP, mito::HyPer2 and mito::pHluorin fluorescence intensity change after laser wounding at time t = 0.

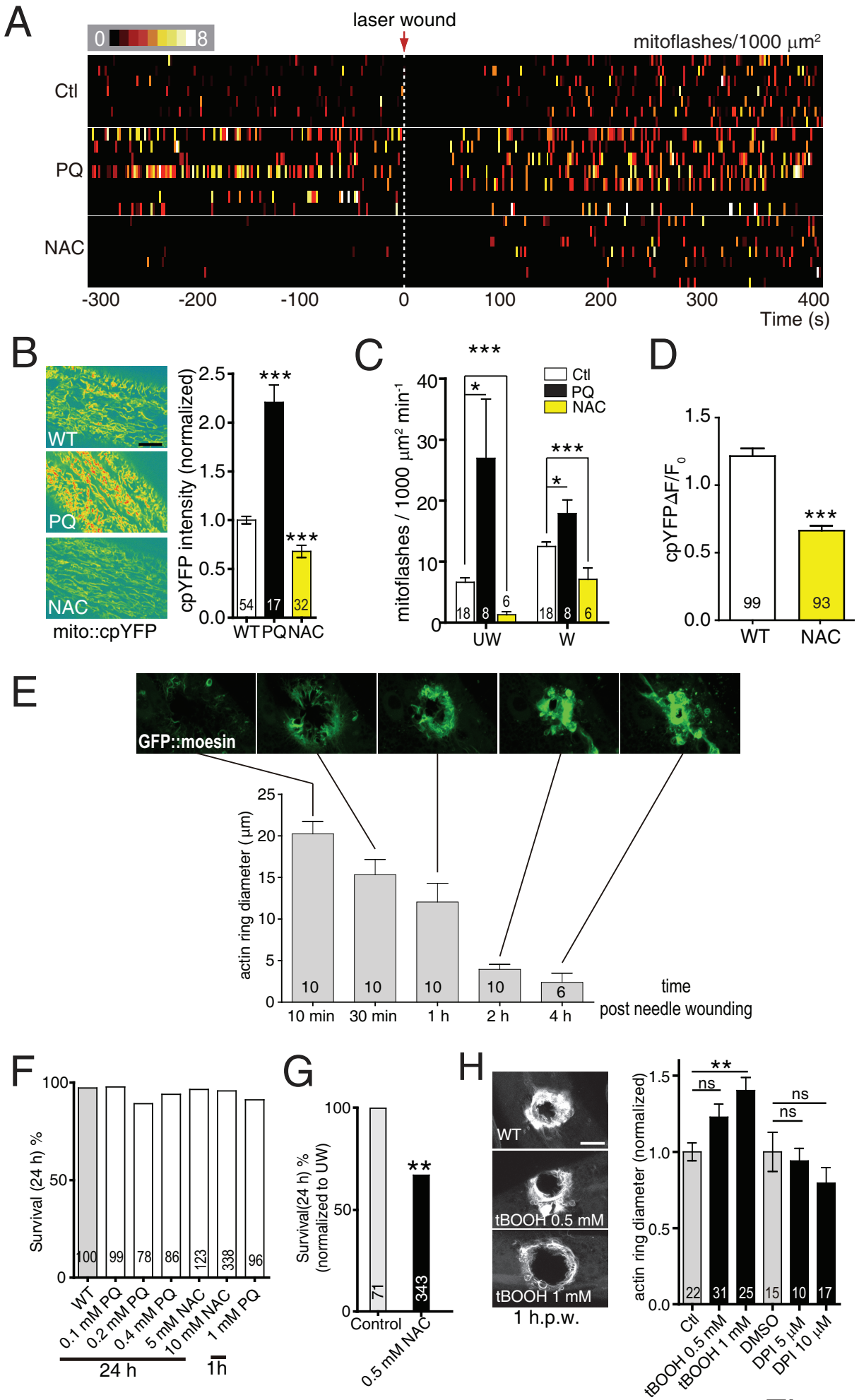
A
laser wound
mitoflashes/1000 μm²
Ctl
PQ
NAC
Time (s)
B
WT
PQ
NAC
mito::cpYFP
cpYFP intensity (normalized)
WT PQ NAC
C
mitoflashes / 1000 μm² min⁻¹
Ctl
PQ
NAC
UW
W
D
cpYFP ΔF/F₀
WT
NAC
E
GFP::moesin
actin ring diameter (μm)
10 min
30 min
1 h
2 h
4 h
time
post needle wounding
F
Survival (24 h) %
WT
0.1 mM PQ
0.2 mM PQ
0.4 mM PQ
5 mM NAC
10 mM NAC
1 mM PQ
24 h
1h
G
Survival(24 h) %
(normalized to UW)
Control
0.5 mM NAC
H
WT
tBOOH 0.5 mM
tBOOH 1 mM
1 h.p.w.
actin ring diameter (normalized)
Ctl
tBOOH 0.5 mM
tBOOH 1 mM
DMSO
DPI 5 μM
DPI 10 μM

Figure S2

Figure S2. The effects of oxidants and antioxidants on wound-induce mtROS production and wound repair, related to Figure 2.

(A) Paraquat (PQ) treatment increases mitoflash frequency and N-Acetyl-Cysteine (NAC) treatment (10 mM) from L4 stage decreases mitoflash frequency in both unwounded and wounded worms at young adult stage; For PQ treatment, worms were transferred into 12 mM levamisole solution with 0.1 mM PQ immediate before imaging and wounding. Heat maps plotted as in Figure 1B.

(B) PQ treatment increased mito::cpYFP fluorescence intensity while NAC treatment decreased mito::cpYFP fluorescence intensity before wounding. Representative confocal images of WT mito::cpYFP and 0.1 mM PQ or 10 mM NAC incubation from L4 stage to young adults; scale, 10 μm. ***, $P < 0.001$, ANOVA. Number of animals indicated in bars in B, C.

(C) Quantitation of mitoflash frequency of WT (control) and worms treated with 0.1 mM PQ or 10 mM NAC shown in panel (A). PQ treatment increased mitoflash frequency before and after wounding in *C. elegans* epidermis while NAC treatment decreases the mitoflash frequency. *, $P < 0.05$, ***, $P < 0.001$, ANOVA.

(D) Quantitation of cpYFP intensity change of mitoflashes in wounded WT and NAC treated worms. Numbers of mitoflashes from a total of 6 worms indicated in bars. ***, $P < 0.001$ (versus control WT), Student's t-test.

(E) *C. elegans* epidermal wound repair by actin assembly after wounding.

Top: Time courses of representative confocal images of F-actin ring around wound site. Scale, 10 μm. Bottom: quantitation of F-actin ring diameter after needle wounding in a time course. In the wild type the actin ring is essentially fully closed by 4 h post

wounding. Actin ring diameter was measured in the same animals at different time points. Number of animals indicated in bars in all panels.

(F) 24 h post-wounding survival ratio of wild type worms treated with different concentrations of Paraquat (PQ) or NAC on NGM plates. Statistics, Fisher's exact test. 24 h: worms cultured on drug plates from L4 stage. 1 h: worms were cultured on drug plates for 1 h before wounding and transferred to normal NGM plates 4 h.p.w.

(G) Survival of needle-wounded wild type (N2) worms in NAC solution. Incubation in 0.5 mM NAC reduces post-wound survival at 24 h. **, $P < 0.01$, Fisher's exact test.

(H) Mimicking increased H_2O_2 levels by treatment with tBOOH (a stable derivative of H_2O_2) from L4 stage slightly inhibits actin ring closure after needle wounding. Reduction in H_2O_2 levels by treatment with DPI, a flavoprotein inhibitor that blocks Nox/Duox dependent H_2O_2 generation, does not significantly affect actin assembly. Note that both tBOOH and DPI affect development if applied at high concentrations from L4 stage. 1 mM tBOOH or 10 μM DPI cause mild developmental defects in young adults after incubation from L4 stage; 0.5 mM tBOOH and 5 μM DPI treated worms appear indistinguishable from DMSO treated controls. **, $P < 0.01$ (versus WT), ANOVA. Scale, 10 μm.

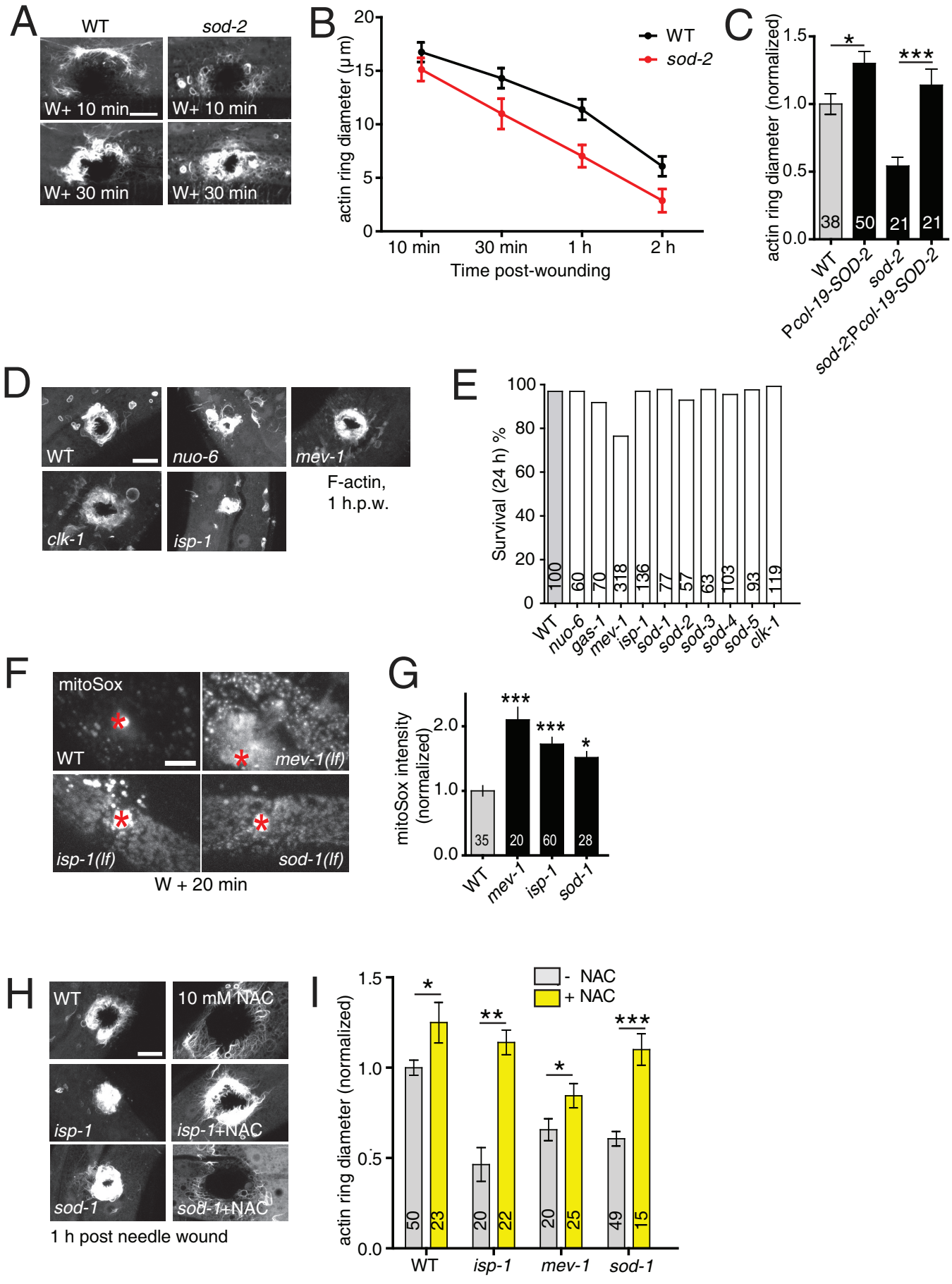
A
WT
sod-2
W+ 10 min
W+ 10 min
W+ 30 min
W+ 30 min
B
actin ring diameter (μm)
Time post-wounding
10 min
30 min
1 h
2 h
WT
sod-2
C
actin ring diameter (normalized)
38
50
21
21
WT
Pcol-19-SOD-2
sod-2
sod-2;Pcol-19-SOD-2
D
WT
nuo-6
mev-1
clk-1
isp-1
F-actin,
1 h.p.w.
E
Survival (24 h) %
100
60
70
318
136
77
57
63
103
93
119
WT
nuo-6
gas-1
mev-1
isp-1
sod-1
sod-2
sod-3
sod-4
sod-5
clk-1
F
mitoSox
WT
mev-1(lf)
isp-1(lf)
sod-1(lf)
W + 20 min
G
mitoSox intensity
(normalized)
35
20
60
28
WT
mev-1
isp-1
sod-1
H
WT
10 mM NAC
isp-1
isp-1+NAC
sod-1
sod-1+NAC
1 h post needle wound
I
- NAC
+ NAC
actin ring diameter (normalized)
50
23
20
22
20
25
49
15
WT
isp-1
mev-1
sod-1

Figure S3

Figure S3. The enhanced wound closure of mitochondrial mutants requires elevated mtROS, related to Figure 3.

(A) Loss of function in *sod-2* causes faster wound closure. Representative confocal images of F-actin assembly at 10 and 30 min after needle wounding. See also Movie S8.

(B) Loss of function in *sod-2* promotes actin ring closure. Quantitation of actin ring diameter at 10 min, 30 min, 1 h, and 2 h post-wounding. n > 20 animals.

(C) Overexpression of SOD-2 in the adult epidermis delays wound closure and rescues enhanced wound closure in *sod-2* mutants. SOD-2 (genomic DNA) was expressed in the adult epidermis under the control of *col-19* promoter. Quantitation of F-actin ring diameter at 1 h.p.w. *, P < 0.01 (versus WT), ***, P < 0.001 (versus *sod-2*), Student's t-test. Number of animals indicated in bars, panels C,E.

(D) Loss of function in mitochondrial ETC genes promotes actin-based wound closure. Representative confocal images of actin assembly around wound site 1 h.p.w.

(E) Mitochondrial mutants display normal 24 h post-wounding survival; Fisher's exact test.

(F) Mutants defective in mitochondrial function show elevated mitoSOX staining after wounding. Representative confocal images of mitoSOX staining in WT, *isp-1*, and *sod-1* mutants 20 min after needle wounding; wounds indicated by red asterisks.

(G) Quantitation of mitoSOX staining intensity, normalized to WT. *, P < 0.05, **, P < 0.01, ***, P < 0.001 (versus WT), one way ANOVA.

(H-I) The accelerated wound closure of mitochondrial mutants is dependent on ROS signals. (H) F-actin ring formation (GFP::moesin) at 1 h.p.w. in mitochondrial mutants, grown on NGM plates with or without NAC (10 mM). Scale (A-C), 10 μm. (I) Quantitation

of actin ring diameter in wounded worms. *, $P < 0.05$, **, $P < 0.01$, ***, $P < 0.001$, versus control (no NAC), Student's t-test.

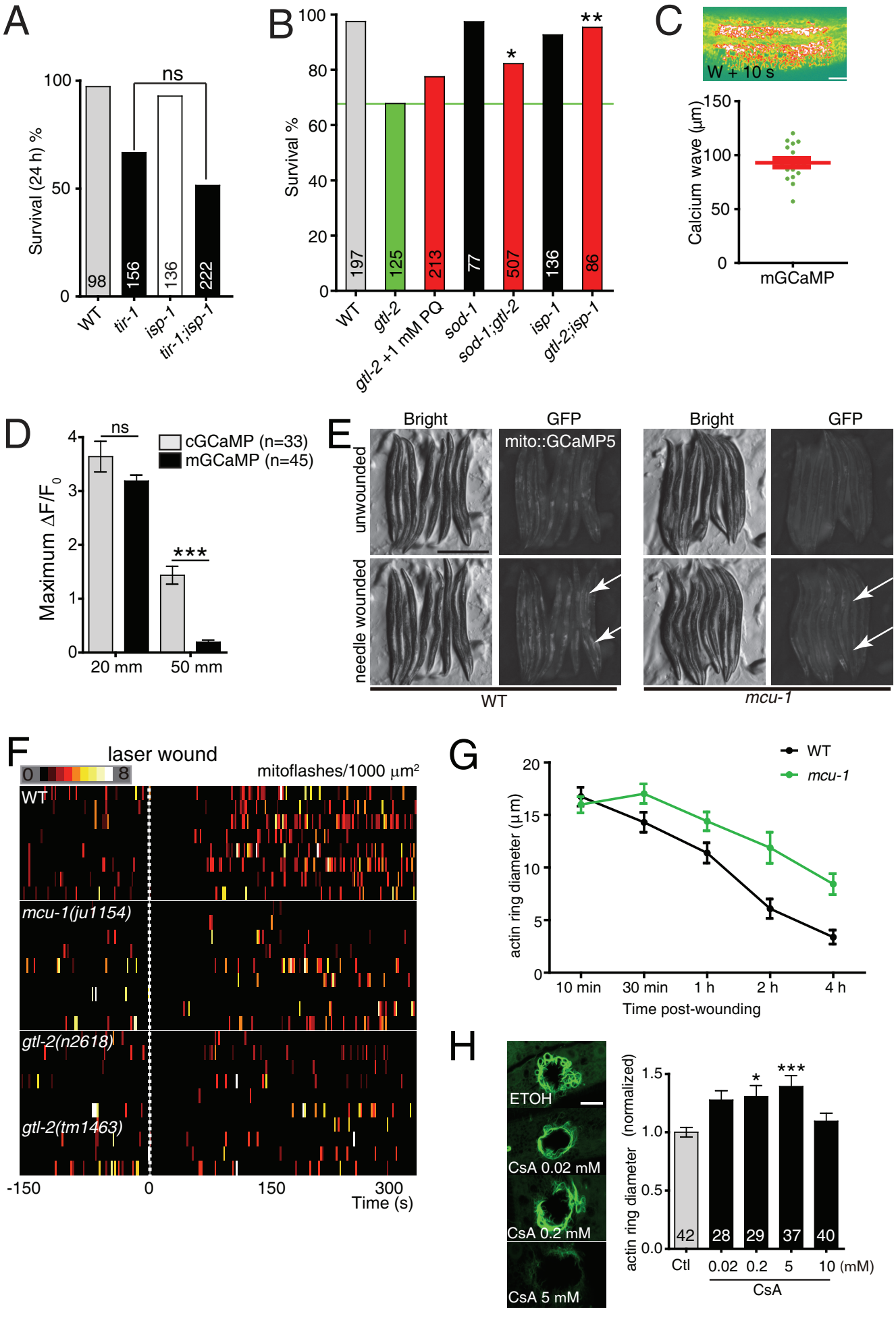
A
Survival (24 h) %
ns
WT
tir-1
isp-1
tir-1;isp-1
B
Survival %
WT
gtl-2
gtl-2 +1 mM PQ
sod-1
sod-1;gtl-2
isp-1
gtl-2;isp-1
C
W + 10 s
Calcium wave (µm)
mGCaMP
D
Maximum ΔF/F0
cGCaMP (n=33)
mGCaMP (n=45)
20 mm
50 mm
E
Bright
GFP
mito::GCaMP5
unwounded
needle wounded
WT
mcu-1
F
laser wound
mitoflashes/1000 µm²
WT
mcu-1(ju1154)
gtl-2(n2618)
gtl-2(tm1463)
Time (s)
G
WT
mcu-1
actin ring diameter (µm)
Time post-wounding
H
ETOH
CsA 0.02 mM
CsA 0.2 mM
CsA 5 mM
actin ring diameter (normalized)
Ctl
CsA

Figure S4

Figure S4 Mitochondrial Ca^{2+} uptake via MCU-1 is required for mitochondrial ROS production and wound closure, related to Figure 4, 5.

(A) The defect in survival after needle wounding of *tir-1* mutants is not suppressed in double mutants with *isp-1*. Number of animals wounded indicated in bars (A, B). Statistics, Fisher's exact test.

(B) The decreased 24 h post-wounding survival of *gtl-2* mutants is suppressed by acute treatment with 1 mM PQ and in double mutants with *sod-1*. *, $P < 0.05$, **, $P < 0.01$, versus *gtl-2.* Fisher's exact test.

(C) The mGCaMP wave spreads up to 50 μm from wound site, n = 18; scale, 10 μm.

(D) Epidermal GCaMP3 fluorescence intensity change is lower at an ROI 50 μm from the wound site compared to an ROI at 20 μm distance; mitochondrial Ca^{2+} uptake is minimal at 50 μm from wound site. ***, $P < 0.001$, Student's t-test.

(E) The mitochondrial Ca^{2+} uniporter MCU-1 is required for mitochondrial Ca^{2+} uptake after needle wounding. Epidermal mitochondrial Ca^{2+} were labeled with *mito::GCaMP5* (*juSi103* transgene). Needle puncture wounds were performed in the anterior and posterior lateral epidermis of young adults. The mito::GCaMP5 signal increased at the wound site in WT animals, but not in *mcu-1* mutants. White arrows mark the wound sites. Scale, 400 μm.

(F) Ca^{2+} signal is required for mitoflash induction after wounding. Heat map shows mitoflash frequency before and after wounding. *gtl-2(n2618 lf)*, *gtl-2(tm1463 null)* and *mcu-1(ju1154)* mutants display reduced mitoflash frequency after wounding.

(G) *mcu-1(ju1154)* mutants display delayed wound closure. Quantitation of actin ring diameter at 10 min, 30 min, 1 h, 2 h, and 4 h post-wounding. n > 15 for each time point; WT wound closure data (10 min – 2 h) are the same as in Figure S5C.

(H) Treatment with the mPTP inhibitor Cyclosporine A (CsA) delays wound closure. WT worms were treated with CsA at different concentrations (20 nM, 200 nM, 2 μM, 5 μM) from L4 stage for 24 h. Control worms were treated with ethanol (0.1 μl per plate). Left, representative confocal image of actin ring 1 h.p.w. Right, quantitation of actin ring diameter, normalized to controls. Scale, 10 μm. Numbers of animals indicated in bars. *, $P < 0.05$, ***, $P<0.01$, ANOVA.

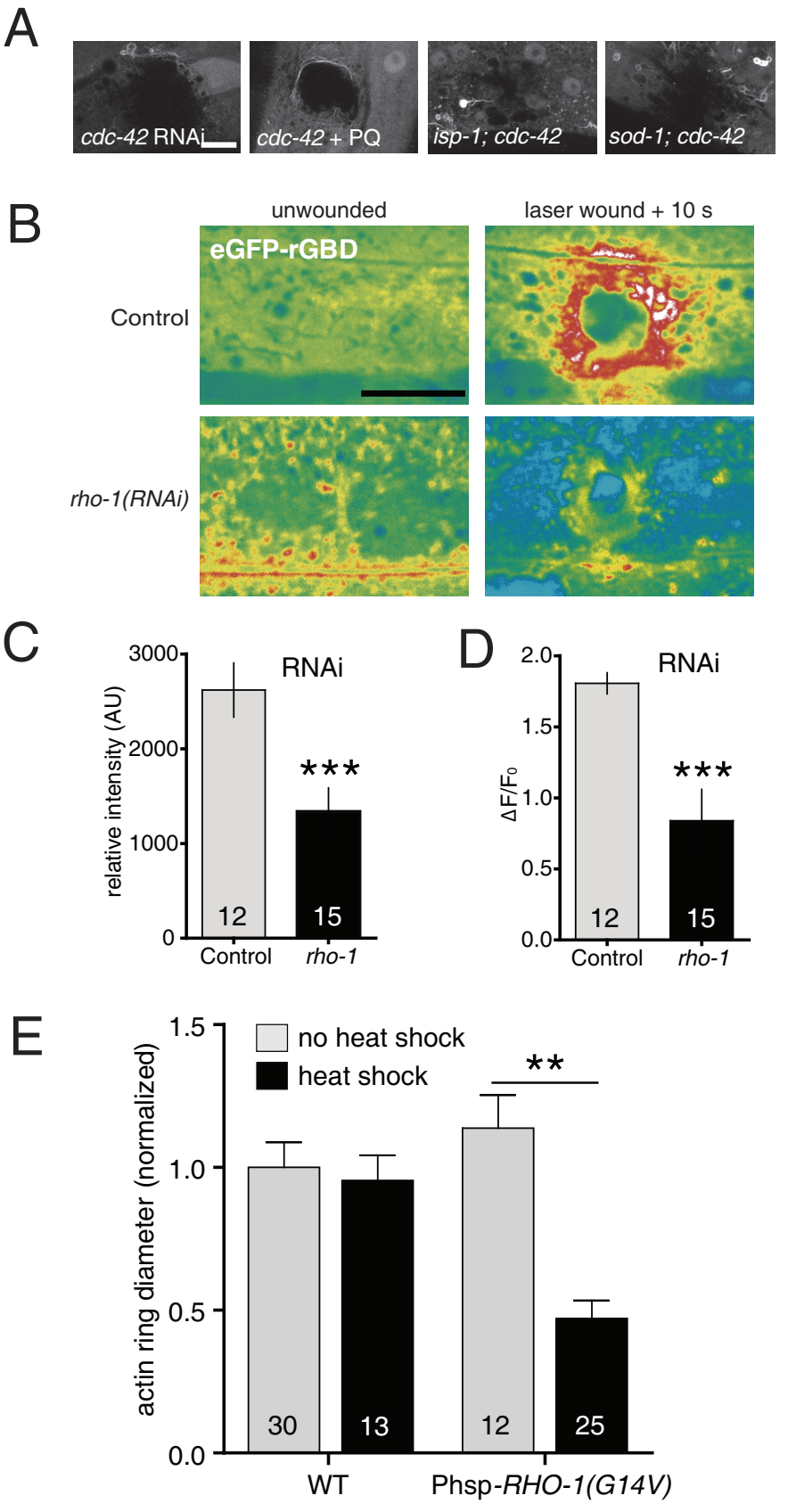
A
cdc-42 RNAi
cdc-42 + PQ
isp-1; cdc-42
sod-1; cdc-42
B
unwounded
laser wound + 10 s
eGFP-rGBD
Control
rho-1(RNAi)
C
RNAi
relative intensity (AU)
3000
2000
1000
0
***
12
15
Control
rho-1
D
RNAi
ΔF/F0
2.0
1.5
1.0
0.5
0.0
***
12
15
Control
rho-1
E
no heat shock
heat shock
actin ring diameter (normalized)
1.5
1.0
0.5
0.0
**
30
13
12
25
WT
Phsp-RHO-1(G14V)

Figure S5

Figure S5. Mitochondrial ROS signals act upstream of the RHO-1 small GTPase in wound repair, related to Figure 6,7.

(A) 0.1 mM PQ treatment from L4 stage does not promote actin-based wound repair in *cdc-42(RNAi)* animals after needle wounding. *cdc-42(RNAi)* also blocks actin assembly in *isp-1* or *sod-1* mutants.

(B) Laser wounding activates RHO-1 in epidermis. Representative confocal images of fluorescence from the genetically encoded Rho sensor eGFP-rGBD. Wounding transiently increases eGFP-rGBD fluorescence intensity around the wound site. The eGFP-rGBD signal is abolished by *rho-1(RNAi)*. Scale (A-B), 10 μm.

(C) *rho-1(RNAi)* decreases baseline eGFP-rGBD fluorescence intensity before wounding. Number of animals indicated in bars (B-D). ***, $P < 0.001$, Student's t-test.

(D) *rho-1(RNAi)* decreases the eGFP-rGBD fluorescence intensity change close to wound site (activation zone) 10 s after laser wounding. ***, $P < 0.001$, Student's t-test.

(E) Constitutively active RHO-1 (caRHO-1) promotes wound closure. caRHO-1 was driven under the control of the heat shock promoter and heat shocked for 2 x1 h heat shock before needle wounding. Quantitation of F-actin ring diameter, normalized to WT. **, $P < 0.01$, Student's t-test.